Optics Letters

Stabilization of passive harmonic mode locking in a fiber ring laser

R. V. Gumenyuk,[1,2] D. A. Korobko,[1,*] and I. O. Zolotovskii[1]

[1]Ulyanovsk State University, 42 Leo Tolstoy Street, Ulyanovsk 432017, Russia
[2]Laboratory of Photonics, Tampere University of Technology, Tampere, Finland
*Corresponding author: korobkotam@rambler.ru

Received 9 October 2019; revised 20 November 2019; accepted 22 November 2019; posted 25 November 2019 (Doc. ID 380064); published 23 December 2019

We propose the model of a harmonically mode-locked soliton fiber ring laser based on the nonlinear polarization rotation taking into account the gain depletion and recovery effects. It is shown that a specific timing jitter could arise in such lasers, since the pulses in the cavity are not strongly identical. To suppress the jitter and stabilize the harmonic mode-locking operation, a method using a small frequency shift followed by the laser radiation filtering is described. The performed numerical simulation shows that the proposed method is able to provide extremely stable harmonic mode locking in a soliton fiber ring laser.

https://doi.org/10.1364/OL.45.000184

Laser sources delivering high-repetition-rate ultrashort pulses are highly demanded in numerous photonic applications [1]. Among them, harmonically mode-locked (HML) soliton fiber lasers exhibiting advantageous consumer properties, such as compactness, reliability, low cost, and ability to maintain convenient output are mostly demanded [2]. Some HML laser configurations compose an intra-cavity filter, such as a high-Q built-in etalon with a free spectral range (FSR) equal to the pulse repetition rate, able to select individual modes from thousands of laser cavity modes to generate multi-gigahertz subpicosecond pulse trains [3]. The disadvantage of this method is the requirement of complex stabilization setups to synchronize the FSR of the etalon with the repetition rate of the laser [4]. Technically, the simplest way to implement HML in a ring fiber cavity is to rearrange the pulses generated through the passive mode locking, making their distribution inside the cavity strongly periodic [5,6]. Passive HML fiber lasers which are able to scale pulse repetition rates up to 20 GHz and more have been reported recently [7,8]. Timing jitter approaching 2% of the interpulse interval and supermode suppression levels (SSLs) varying within a wide range from −15 to −60 dB and below [8–10] are considered to be typical indicators of the stability of the operation achieved with the HML lasers.

It is commonly accepted that a regular temporal pattern of HML formed in a fiber ring laser is induced by the repulsion forces between the pulses [5,6]. However, the physics of this interaction is not clear in detail. The interaction between pulses can include repulsion between antiphase pulses, interaction through saturating and relaxing dissipative parameters [11], and interaction through acoustic waves induced by electrostriction [12]. Besides, the role of a continuous-wave (CW) component of the optical spectrum in HML is still under discussion. It was theoretically demonstrated that a CW component acts as an efficient agent to manage the interaction between neighboring pulses. It has also been reported independently that a low power external CW does not have a major impact on the stability of the harmonic mode-locking distribution, thus highlighting the robustness of an initial state HML against the external injection [13,14].

In this Letter, we try to emphasize the possible complexity of stable HML and assume that its stabilization is provided by a cooperative action of several mechanisms. This assumption is encouraged by the results of a report on a Tm-Ho fiber ring laser with a hybrid mode locking combining the frequency-shifted feedback (FSF) and nonlinear polarization rotation (NPR) [9]. The laser ring cavity composes segments of active and passive single-mode fibers (SMFs) exhibiting a total anomalous dispersion. An acousto-optic shifter with a frequency shift about 40 MHz is also included in the cavity. Near the lasing threshold the laser generates subpicosecond soliton pulses with the fundamental frequency of 29.2 MHz. When the pump is increased, the laser starts to operate in a HML regime, demonstrating effective suppression of the supermode noise. The results of the laser operation at the repetition rate of 409.4 MHz (14th harmonic of the cavity) and with a SSL below −66 dB are shown in Fig. 1(a) [9]. With an increase in the cavity length and decrease of the fundamental frequency down to 12.4 MHz, a stable HML operation is maintained. For laser operating at 1 GHz (81st harmonic of the longer cavity), the SSL is about −60 dB [Fig. 1(b)].

Further, we explore and describe the physical mechanism responsible for extremely stable operation in the HML lasers. The fact that a stable HML regime in Ref. [9] is available for a wide range of repetition rates and cavity lengths excludes consideration of the transverse acoustic wave excitation mechanism as a mechanism responsible for laser stabilization [15]. The mechanism of HML stabilization associated with a separate CW component is also excluded due to the absence of this component in the laser optical spectrum. As a result, the repulsion

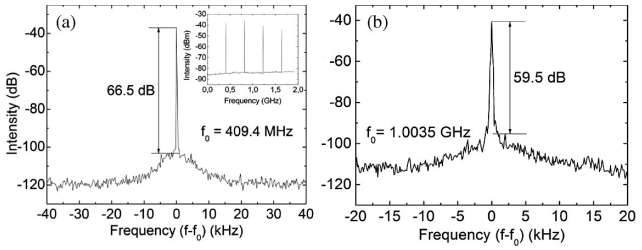

Fig. 1. RF spectrum of a HML Tm-Ho fiber ring laser with FSF. (a) Harmonic mode-locked operation showing the 14th harmonic of the cavity (fundamental frequency is 29.2 MHz). Inset: the RF spectrum with a 2.0 GHz bandwidth [9]. (b) Same for the 81st harmonic of the laser with the longer cavity. (The fundamental frequency is 12.4 MHz.)

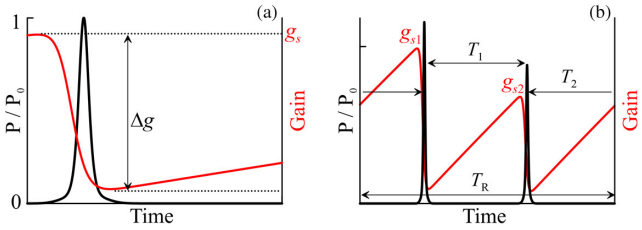

Fig. 2. (a) Scheme of the time-dependent gain across an amplified soliton pulse. (b) Scheme of interaction through GDR in the cavity with a period $T_R = T_1 + T_2$. (T_1, T_2 are the time intervals between the pulses.)

of pulses through the gain depletion and recovery (GDR) [16] remains the only mechanism responsible for pulse interaction.

Qualitatively, the laser gain is depleted while transferring energy to a traversing pulse. As a result, the pulse experiences a time-dependent gain, i.e., the leading edge of the pulse sees a larger gain than the trailing edge [Fig. 2(a)]. The pulse with group velocity $v_g^{-1} = dt/dz$ under such a condition acquires group-velocity drift towards the region of higher gain. Denoting the gain depletion during interaction with the pulse as Δg, it can be shown that this group-velocity drift is proportional to the value of Δg [16].

The GDR is described by the standard rate equation

$$\frac{dg_s}{dt} = \frac{g_{s0} - g_s}{\tau_g} - \frac{g_s |A(z,t)|^2}{E_g}. \quad (1)$$

Here g_{s0} is the unsaturated gain, and E_g is the gain saturation energy. Assuming that the energy E_s of the pulse is low compared to the value of E_g, gain depletion can be expressed as $\Delta g = g_s E_s / E_g$, where g_s corresponds to the value of the gain just before the arriving of the pulse. If the laser cavity contains several pulses, then the GDR effect leads to their mutual repulsion. Let us analyze this interaction in more detail. For simplicity, we consider the case of two pulses. However, generalization for an arbitrary number of pulses could be also implemented. The used terms are illustrated in Fig. 2(b). A change of the time intervals between pulses is proportional to the difference in the group-velocity drifts:

$$\frac{d(T_1 - T_2)}{dz} = \Delta g_1 - \Delta g_2. \quad (2)$$

At the same time, in linear approximation for relaxation valid at $\mu = T_R/\tau_g \ll 1$, the gain depletions and interpulse distances are connected by the next equations:

$$\frac{E_g}{E_{s\,3-i}} \Delta g_{3-i} - \frac{E_g}{E_{s\,i}} \Delta g_i + \Delta g_i = \mu T_i, \quad i = 1, 2. \quad (3)$$

Assuming that the pulse energies E_{si} are equal for all pulses, Eqs. (2) and (3) yield

$$\frac{d(T_1 - T_2)}{dz} = -\frac{\mu}{2E_g/E_s - 1}(T_1 - T_2) = -\alpha(T_1 - T_2), \quad \alpha > 0. \quad (4)$$

Thus, the initial difference of time intervals tends to zero exponentially: $(T_1 - T_2) = (T_1 - T_2)_0 \exp(-\alpha z)$, ensuring an equidistant pulse arrangement inside the cavity. This arrangement is stable, since any fluctuation of $|T_1 - T_2| > 0$ decreases with the same decrement α. However, a deeper analysis shows that the higher integral gain $\int_0^L g_{si}(z)dz$ corresponds to the higher pulse energy E_{si} [Fig. 2(b)]. Thus, the assumption about equality of the pulse energies is not precisely true, and the pulse train possesses intensity jitter. Denoting the difference of the pulse energies as $E_{s1} - E_{s2} = \Delta(z) > 0$, Eq. (4) describing evolution of the interpulse distances can be expressed as

$$\frac{d(T_1 - T_2)}{dz} = -\alpha(T_1 - T_2) - \frac{\mu}{2E_g} \Delta(z)\, T_2(z). \quad (5)$$

In this case, the equidistant pulse arrangement $T_1 = T_2$ no longer corresponds to the stationary point of Eq. (5). Assuming that $\Delta/E_g \ll 1$ is a small random variable, we obtain that the uniform pulse arrangement due to GDR is accompanied by random changes in the interpulse distances referred to as the timing jitter of a pulse train. There are several sources of timing jitter in mode-locked lasers: pump power fluctuations, various thermal effects, and noise of the laser gain medium. An HML fiber laser has an additional source of the timing jitter owing to the uncontrollable changes of adjacent pulse temporal positions and, hence, this jitter is significantly stronger than the jitter in lasers operating the fundamental frequency [15]. The case described by Eq. (5) exactly belongs to this type of timing jitter specific for HML lasers. We will consider the means of suppression of this jitter providing stability to the pulse train comparable with the laser operating fundamental frequency.

Obviously, the simplest way to suppress the jitter is to eliminate the pulse energy difference Δ. For this, the method of sliding-frequency filters proposed for soliton transmission lines [17,18] could be used. However, in the considered case, this mechanism is used to stabilize the hybrid mode-locking scheme. Its action is based on the fact that soliton pulses of different energies also differ in group velocities and frequencies. Let us explain this process, following the scheme depicted in Fig. 3. We consider the case when the solitons are almost periodically arranged along the cavity $T_1 \approx T_2$, wherein the difference in velocities dt_i/dz is mainly determined by the difference in soliton energies E_{si} (providing the velocity drift $\propto g_s E_s / E_g$). An example of change in the soliton velocities is shown in Fig. 3(a). Here the energy of the second soliton is higher than that of the first soliton $E_2(z) > E_1(z)$ along the whole segment z. Using the Taylor expansion, the soliton velocities can be expressed

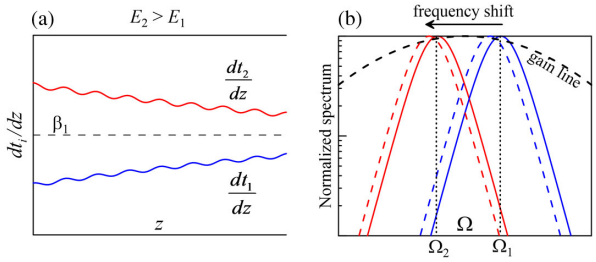

Fig. 3. (a) Change in the velocities dt_i/dz of solitons with different energies. (b) Equalization of soliton energies using the frequency shift.

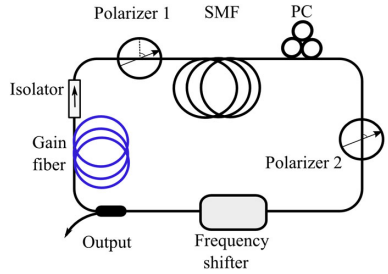

Fig. 4. Fiber ring laser configuration used in the numerical simulation.

in terms of the total average velocity $(\bar{v})^{-1} = \beta_1$ and soliton frequencies:

$$dt_i/dz \approx \beta_1 + \beta_2\,(\omega_i\,(z) - \omega_0) = \beta_1 + \beta_2 \Omega_i\,(z)\,,$$

where ω_0 is the carrier frequency, and ω_i, Ω_i are the pulse frequencies. Hence, at anomalous group-velocity dispersion (GVD) $\beta_2 < 0$ a soliton of higher energy has a lower frequency, and vice versa [Fig. 3(b)].

To equalize energies, the FSF method employs the spectral filtering effect. In general, a special filter can be used for this, but we consider the model case of a spectrally limited gain. Figure 3(b) shows that at a leftward frequency shift $\Omega' = \Omega + 2\pi f$, $f < 0$, and the lower frequency pulse experiences the gain less than the pulse with frequency $\Omega_1 > \Omega_2$. As a result, the pulse energies and, consequently, the pulse velocities and frequencies are equalized. This mechanism is stable and selective, i.e., the pulse with the lower energy always acquires the higher gain. When one pulse acquires higher energy than the other, its velocity dt_i/dz increases, and its frequency shifts leftward from the gain peak to an energetically unfavorable frequency domain. It is worth nothing that the rightward frequency shift $f > 0$ has an opposite effect. Higher energy solitons acquire a higher gain, while lower energy pulses gradually degenerate. As a result, the harmonic arrangement of pulses over the cavity is destroyed. The proposed model is applicable to the cases when there is only one mechanism associated with GDR which is responsible for HML establishment. The effectiveness of this mechanism is determined by the ratio of the gain recovery timescale to the interpulse spacing, and it decreases with an increasing pulse repetition rate. Thus, at a high repetition rate (> 10 GHz), the proposed mechanism is effective only for pulses of sufficiently high energy depleting the gain significantly.

To verify this mechanism, a numerical simulation of a soliton ring fiber laser with GDR was performed. The laser configuration is shown in Fig. 4.

We assume that the radiation propagating in the gain fiber is linearly polarized, and it is elliptically polarized propagating in a SMF. The SMF has negligibly low birefringence, and a mode-locking effect occurs in accordance with the model [19].

The field propagation in the gain fiber is described by the Ginzburg–Landau equation

$$\frac{\partial A}{\partial z} - i\frac{\beta_{2g}}{2}\frac{\partial^2 A}{\partial t^2} - i\gamma_g |A|^2 A = \frac{gA}{2} + \frac{\beta_{2f}}{2}\frac{\partial^2 A}{\partial t^2},$$

where z is the coordinate along the fiber, β_{2g} is the GVD, and γ_g is the Kerr nonlinearity of the gain fiber. To simplify the simulation, the gain is divided into two parts: $g(z,t) = g_n(z) + g_s(z,t)$, $g_n \gg g_s$. The first term responsible for major contribution to the gain is time-independent. Thus, it can be averaged over the simulation window as

$$g_n(z) = g_{n0}\left(1 + \frac{1}{E_g}\int_0^{\tau_{\text{win}}} |A(z,t)|^2 \mathrm{d}t\right)^{-1},$$

where E_g is the gain saturation energy, and τ_{win} is the size of simulation window. The second part corresponds to GDR, and it is described by Eq. (1). The gain spectral filtering is employed in parabolic approximation $\beta_{2f} = (g_n - \bar{g}_s)/\Omega_g^2 \approx g_n/\Omega_g^2$, where Ω_g is a HWFM gain line bandwidth, and the overbar indicates averaging over the simulation window. The light propagation in the SMF is described by two coupled nonlinear Schrödinger equations:

$$\frac{\partial A_j}{\partial z} - i\frac{\beta_2}{2}\frac{\partial^2 A_j}{\partial t^2} - i\gamma\left(|A_j|^2 + \frac{2}{3}|A_{3-j}|^2\right)A_j$$

$$-\frac{i}{3}\gamma A_j^* A_{3-j}^2 = 0, \quad j = 1, 2,$$

where β_2 is the GVD, and γ is the Kerr nonlinearity coefficient in the SMF. The amplitudes A_j are determined by Polarizer 1 as $A_1 = A\cos\varphi_1$, $A_2 = A\sin\varphi_1$, the polarization controller tunes the polarization angle as $A_2 = A_2 \exp i\theta$, and Polarizer 2 restores the original state of polarization $A = A_1\cos\varphi_2 + A_2\sin\varphi_2$. The fiber lengths are $l_g = 2.5$ m for the gain fiber and $l_{\text{SMF}} = 5$ m for the SMF. The periodic boundary conditions are applied, i.e., the simulation window corresponds to the cavity period $\tau_{\text{win}} = T_R = T_1 + T_2$. The frequency shifter and output coupler are accounted for in the transfer functions $A'(\Omega) = A(\Omega - 2\pi f)$ and $T_c \equiv A'/A = 0.95$. The frequency shift corresponds to the step of the frequency grid $2\pi f = 1/T_R$. The main parameters of the model are listed in Table 1. We should note that the values of τ_g and T_R corresponding to real lasers are 1000 times more but, to accelerate the simulation process, these values are chosen to be sufficiently small. They fully satisfy the necessary condition $T_R \ll \tau_g$, and the simulation provides an adequate description of the pulse interaction in the cavity. Two identical pulses exhibiting a small deviation from the equidistant arrangement $|T_1 - T_2| = 1$ ps are chosen as initial conditions. The simulation results are shown in Fig. 5. Note that a cyclic shift of the simulation window has been periodically applied.

First, we consider the model that does not use the frequency shifter [Figs. 5(a)–5(c)]. The simulation results show that the conditions for amplification of pulses are not completely equivalent. Initially, the same pulses acquire unequal energies with

Table 1. Parameters of the Simulation

Parameter	Value	Parameter	Value
γ, γ_g (W^{-1} m^{-1})	0.0033	E_g (pJ)	30
β_2, β_{2g} (ps^2 m^{-1})	−0.018	T_R (ps)	19.2
Ω_g (ps^{-1})	0.3	τ_g (ps)	300
g_{n0} (m^{-1})	1.5	g_{s0} (m^{-1})	0.1
φ_1, φ_2	$\pi/8, \pi/2$	θ	$3\pi/4 - 0.25$

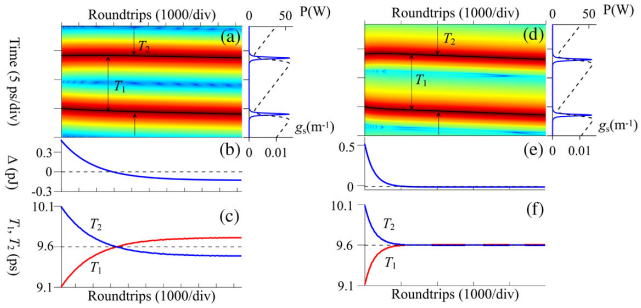

Fig. 5. (a)–(c) Simulation without the frequency shifter. (a) Evolution of the pulse arrangement inside the cavity. Right: the final arrangement of the pulses and GDR distribution. (b) Change of the pulse energy difference. (c) Evolution of the interpulse distances. (d)–(f) Same as in (a)–(c), but with the frequency shifter.

the difference of about 0.5 pJ due to difference in the GDR values. Then, during the interaction, the interpulse distances are equalized and the value of Δ decreases. However, after 10^4 round-trips, it is about 1% of the single pulse energy. Finally, in the system without a frequency shifter, the pulse interaction through the GDR leads to the pulse arrangement in the cavity that differs from the HML equidistant distribution by significant timing jitter $|T_2 - T_1| \approx 0.25$ ps, which is more than 2.5% of the interpulse distance. The frequency shifter included in the system [Figs. 5(d)–5(f)] allows reducing the pulse energy difference down to nearly 0 for 1000 round-trips, thereby leading to total suppression of the timing jitter $T_2 = T_1 = T_R/2$ and stable harmonic mode locking.

As mentioned above, the considered HML stabilization method can be referred to as hybrid mode locking combining the FSF and NPR techniques. Importantly, in the proposed configuration, pulse mode locking occurs due to the NPR mechanism alone. The role of the FSF is a non-destructive pulse perturbation, leading only to the small frequency shift inside the spectral filter. In the proposed model, any small frequency shift leads to stabilization of the equidistant pulse arrangement achieved through GDR. The shift increase leads to a faster stabilization dynamics. However, it is worth noting that a system with the fixed parameters and given initial conditions is characterized by a certain threshold shift value providing HML stabilization. Exceeding this threshold value can break the dissipative balance and decrease the number of pulses. The proposed scheme of timing jitter suppression for a system with the GDR can be generalized for an arbitrary number of soliton pulses, since the dependence of the pulse frequency on its energy is extended to this case as well.

In conclusion, in this Letter, the soliton fiber ring laser with the passive HML has been considered. Here the GDR is proposed as the pulse interaction mechanism ensuring a uniform distribution of the pulses inside the cavity. It is shown that the HML associated with such a mechanism causes the loss of identity of the pulses in the train, thus provoking timing jitter. To suppress the jitter, we propose a method to stabilize HML operation employing a small frequency shift followed by spectral filtering.

Funding. Russian Science Foundation (19-72-10037); Russian Foundation for Basic Research (18-42-732001).

Disclosures. The authors declare no conflicts of interest.

REFERENCES

1. A. Schliesser, N. Picqué, and T. W. Hänsch, Nat. Photonics **6**, 440 (2012).
2. M. E. Fermann and I. Hartl, Nat. Photonics **7**, 868 (2013).
3. D. A. Korobko, A. A. Fotiadi, and I. O. Zolotovskii, Opt. Express **25**, 21180 (2017).
4. G. Sobon, K. Krzempek, P. Kaczmarek, K. M. Abramski, and M. Nikodem, Opt. Commun. **284**, 4203 (2011).
5. X. Liu and M. Pang, Laser Photonics Rev. **13**, 1800333 (2019).
6. A. B. Grudinin and S. Gray, J. Opt. Soc. Am. B **14**, 144 (1997).
7. H. Chen, S. P. Chen, Z. F. Jiang, and J. Hou, Opt. Express **23**, 1308 (2015).
8. C. Lecaplain and P. Grelu, Opt. Express **21**, 10897 (2013).
9. T. Noronen, O. Okhotnikov, and R. Gumenyuk, Opt. Express **24**, 14703 (2016).
10. A. I. Trikshev, V. A. Kamynin, V. B. Tsvetkov, and P. A. Itrin, Quantum Electron. **48**, 1109 (2018).
11. D. A. Korobko, O. G. Okhotnikov, and I. O. Zolotovskii, Opt. Lett. **40**, 2862 (2015).
12. E. M. Dianov, A. V. Luchnikov, A. N. Pilipetskii, and A. N. Starodumov, Opt. Lett. **15**, 314 (1990).
13. G. Semaan, A. Komarov, M. Salhi, and F. Sanchez, Opt. Commun. **387**, 65 (2017).
14. A. Komarov, K. Komarov, A. Niang, and F. Sanchez, Phys. Rev. A **89**, 013833 (2014).
15. S. Gray, A. B. Grudinin, W. H. Loh, and D. N. Payne, Opt. Lett. **20**, 189 (1995).
16. J. N. Kutz, B. C. Collings, K. Bergman, and H. Knox, IEEE J. Quantum Electron. **34**, 1749 (1998).
17. A. Mecozzi, J. D. Moores, H. A. Haus, and Y. Lai, J. Opt. Soc. Am. B **9**, 1350 (1992).
18. O. Yushko, A. Redyuk, M. Fedoruk, K. J. Blow, N. J. Doran, A. D. Ellis, and S. Turitsyn, Opt. Lett. **39**, 6308 (2014).
19. C.-J. Chen, P. K. A. Wai, and C. R. Menyuk, Opt. Lett. **17**, 417 (1992).